MRS Communications (2015), *5*, 565–571

doi:10.1557/mrc.2015.75

MRS Communications

Plasmonics, Photonics, and Metamaterials Research Letter

Nonlinear nanocircuitry based on quantum tunneling effects

Pai-Yen Chen, Department of Electrical and Computer Engineering, Wayne State University, Detroit, Michigan 48202, USA
Khai Q. Le, Department of Electrical Engineering, University of Minnesota, Duluth, Minnesota 55812, USA; Faculty of Science and Technology, Hoa Sen University, Ho Chi Minh, Vietnam
Andrea Alù, Department of Electrical and Computer Engineering, University of Texas at Austin, Austin, Texas 78712, USA

Address all correspondence to Pai-Yen Chen at **pychen@wayne.edu** and Andrea Alù at **alu@mail.utexas.edu**

(Received 16 September 2015; accepted 20 November 2015)

Abstract

Metatronics, or metamaterial-inspired optical nanocircuitry, has provided a powerful toolset to tailor and implement modular quasi-static circuit functionalities in the optical regime. So far, these concepts have been mostly limited to linear operations, while many of the relevant operations in integrated circuits require nonlinear responses. In this work, we introduce nonlinear infrared nanocircuit elements exploiting large quantum conductance driven by photon-assisted tunneling and enhanced by hybrid plasmonic nanojunctions. Based on these concepts, we present infrared lumped nanocircuit mixers and switches for second-harmonic generation, and wide-spectrum self-amplitude modulators based on nanorods.

Metatronic circuitry has emerged as a promising technology platform for the development of high-throughput integrated optical circuitry for processing photons using parameterized and modular circuit elements, namely resistors (R), capacitors (C), and inductors (L), in analogy with conventional radio-frequency (RF) microelectronic circuitry,[1–5] but with the promise of operating at much smaller and faster scales in the infrared (IR) and visible regimes. Different from their RF counterparts, the non-negligible electric field inside dielectric/metallic (plasmonic) nanoparticles is responsible for the flow of an optical displacement current density,[5] which plays a significant role, more relevant than the conduction current density, which dominates at lower frequencies, i.e., RF and microwaves. The optical input impedance of an arbitrary nanoparticle can be defined, consistently to the conventional impedance of an RF circuit element, as the ratio between the average potential difference at its terminals and the optical displacement current across it.[6] Following this definition, the concept of metamaterial-inspired optical nanocircuitry was first introduced in[1,2] based on nanoparticles with plasmonic [negative real part of permittivity, $\mathrm{Re}(\varepsilon) < 0$] and dielectric [positive real part of permittivity, $\mathrm{Re}(\varepsilon) > 0$] materials, respectively acting as nanoinductors and nanocapacitors for optical fields. The non-zero imaginary part of permittivity [$\mathrm{Im}(\varepsilon) \neq 0$] can synthesize a localized nanoresistor. The combination of optical lumped elements may offer wide possibilities to build nanocircuits for numerous optical applications. Recently, passive metatronic circuitries have been experimentally demonstrated, with applications ranging from stereo bandpass and bandstop nanofilters,[3,4] to tuning and matching nanoantennas,[7–9] to higher-order circuitry made of complex clusters of resonant nanoparticles.[10,11] However, to bring these nanocircuits to the functional level of RF microelectronic circuits, active and nonlinear elements must be explored. The overarching goal of this work is to enrich the concept of metatronics by introducing nonlinear mixing and modulation at IR wavelengths using modular nanocircuit elements.

Modern communication schemes typically require nonlinear and active components for amplitude and frequency modulation, demodulation, and multiplexing.[12] For instance, frequency mixers are nonlinear circuit elements commonly used to upconvert and/or downcovert the input signal into orthogonal high-/sub-harmonic output signals.[12] As another example, all-optical switching relies on nonlinear self-amplitude modulation, as a self-action of intense pulsed light. Recently, nonlinear metatronic elements have been proposed using subwavelength plasmonic junctions, e.g., a metallic dipole nanoantenna loaded with nonlinear optical materials.[13–23] Surface plasmon resonances, as a coherent excitation of conduction-band free electrons, may substantially enhance the local field intensity in the vicinity (particularly in the gap region) of plasmonic nanostructures, thereby boosting otherwise weak optical nonlinearities. Several nonlinear elements for IR and optical circuitry have been proposed to realize specific nonlinear functions, such as phase conjugation,[14] difference frequency generation,[18] frequency multiplication, all-optical bistable switching,[13,20], and spatial multiplexing,[21] as well as diode[24] and transistor[25] functionalities within the metatronics paradigm. However, these nonlinear elements necessitate proper loading of nonlinear nanoparticles (e.g., epitaxial III–V compounds), accurate fabrication of complicated geometry (e.g., isolated nanostructure arrays), and integration. In the following,

we propose and theoretically investigate an effective layout for nonlinear metatronics, achieving subwavelength IR elements with large nonlinear response in a simple planarized geometry.

The geometry of interest, shown in Fig. 1(a), is formed by dissimilar plasmonic junctions of periodic silver (Ag)-tantalum pentoxide (Ta_2O_5)-gold (Au) films. We also study a higher-order nanocircuit, shown in Fig. 1(b), where the transverse gaps as shunt nanocapacitors may provide more flexibility in tuning frequency responses. The corresponding nanocircuit models for these metatronic devices are shown in Figs. 1(c) and 1(d). Using an atomic scale Ta_2O_5 insulating layer, which can be precisely controlled by atomic-layer deposition, the quantum conductance due to multiphoton-assisted electron tunneling through a metal–oxide–metal (MOM) nanojunction may be controlled.[26–33] This quantum conductance has nonlinear components, effectively introducing a nonlinear nanoresistor in parallel to the nanocapacitor formed by the MOM structure. Indeed, it has been recently observed experimentally and studied theoretically that the power dissipation due to quantum conductance may set an upper limit to the quality factor and maximum possible field enhancement in plasmonic nanostructures.[26,29–32] When an intense pulsed laser illuminates the IR nanocircuit of Fig. 1, within the quantum mechanical regime, the photon-assisted tunneling (PAT) process can induce

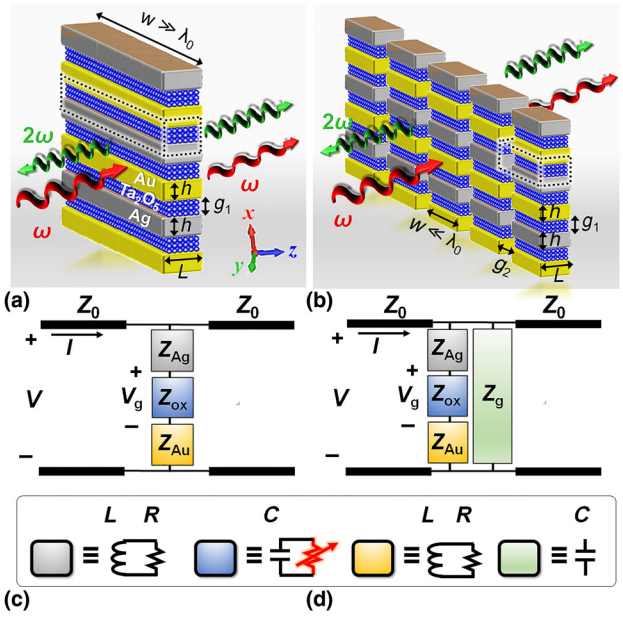

Figure 1. Schematic diagrams of: (a) a metatronic circuit made of periodic dissimilar plasmonic nanojunctions, (b) a higher-order circuit obtained adding shunt air-gap capacitances. Panels (c) and (d) are the corresponding nanocircuit models. The electric field is perpendicular to the semi-infinite nanorods (*x*-axis), forming a series combination of lumped circuit elements. After considering the quantum effect of multiphoton-assisted tunneling, flatland nanocircuits made of dissimilar MOM superlattices can exhibit efficient nonlinear optical effects.

relevant second-order and other higher-order nonlinearities in dissimilar MOM junctions, enabling a variety of nonlinear optical functions, such as rectification,[33] second-/third-harmonic generation,[30] and two-photon absorption (TPA).[29–32]

Assuming an $e^{-i\omega t}$ time-harmonic dependence for the structure in Fig. 1(a), when the IR electric field is perpendicular to the *x*-axis, the proposed geometry operates as a series combination of lumped impedances $Z_{Ag} = (ih)/(2\varepsilon_{Ag}\varepsilon_0\omega wL)$, $Z_{Au} = (ih)/(2\varepsilon_{Au}\varepsilon_0\omega wL)$, and $Z_{ox} = (ig_1)/(\varepsilon_{T_2O_5}\varepsilon_0\omega wL)$, which result in an equivalent surface impedance $Z_{eq} = Z_{Au} + Z_{Ag} + Z_{ox}$, where ε_0 is the free-space permittivity, w and L are the width and length of the semi-infinite metal and oxide nanostrips, h and g_1 are the thickness of metal nanostrips and oxide films [see Fig. 1(a)]. The relative permittivities of Au and Ag, $\varepsilon_{Au}(\omega)$ and $\varepsilon_{Ag}(\omega)$, are assumed to follow a Drude-type dispersion,[34,35] (Below the onset of metal's interband transition, the relative permittivity of metal following the Drude-type dispersion model: $\varepsilon_m = \varepsilon_\infty - \omega_p^2/[\omega(\omega + i\gamma)]$, where the empirical parameters for Au are $\omega_p/2\pi = 2449$ THz, $\gamma/2\pi = 16.68$ THz and $\varepsilon_\infty = 6.9$, and those for Ag are $\omega_p/2\pi = 2221$ THz, $\gamma/2\pi = 4.83$ THz and $\varepsilon_\infty = 3.7$) and in the IR region the relative permittivity of Ta_2O_5, $\varepsilon_{Ta_2O_5} = 4.4$.[36] From the lumped element circuit model in Fig. 1(a), the transmittance of incident optical signals can be calculated as $T = tt^*$ with the complex transmission coefficient $t = Z_{eq}/(Z_{eq} + Z_0/2)$, where $Z_0 = \eta_0(g_1 + h)/w$ and $\eta_0 = 377\ \Omega$ (wave impedance of free-space). The transmittance of the higher-order circuit in Fig. 1(b) can be similarly obtained by modifying the characteristic impedances to $Z_0 = \eta_0(g_1 + h)/(g_1 + w)$ and $Z_{eq} = [(Z_{Au} + Z_{Ag} + Z_{ox})^{-1} + Z_g^{-1}]^{-1}$, where the capacitive air-gap impedance $Z_g = i(g_1 + h)/(\varepsilon_0\omega g_2 L)$.

Figures 2(a) and 2(b) compare the transmission coefficients and the electric field enhancement factor inside the MOM nanojunction (neglecting quantum nonlocal effects[37]) for the structure in Fig. 1(a), with geometric parameters $L = 10$ nm, $g_1 = 0.8$ nm, and h (15, 20, 30, 40 nm). Results calculated using the metatronic circuit theory and full-wave simulations are shown with lines and dots, respectively. It is clear that IR band-notch filters can be quantitatively designed using the circuit approach, in analogy with.[3] Since the electric field is approximately uniform in the oxide region,[3,4] the electric field enhancement factor inside the MOM nanojunctions can be calculated using the circuit model in Fig. 1(c) as the voltage drop across the oxide impedance divided by the oxide thickness (e.g., $E_g = V_g/g_1$). The analytical circuit model well describes the structure, provided that the dimensions of metallic and oxide nanostrips are subwavelength. Figs. 2(c) and 2(d) refer to the nanocircuit in Fig. 1(b) with different widths of the air gap, which affects the shunt impedance Z_g (solid and dashed lines correspond to $h = 15$ nm and $h = 40$ nm). Here a non-negligible parasitic capacitance $Z_{par} = 0.2\ Z_{ox}$ in parallel to Z_{ox} (due to the effect of fringing fields in the air region), with its value extracted from full-wave simulations, was introduced to improve the accuracy of our analytical model. By

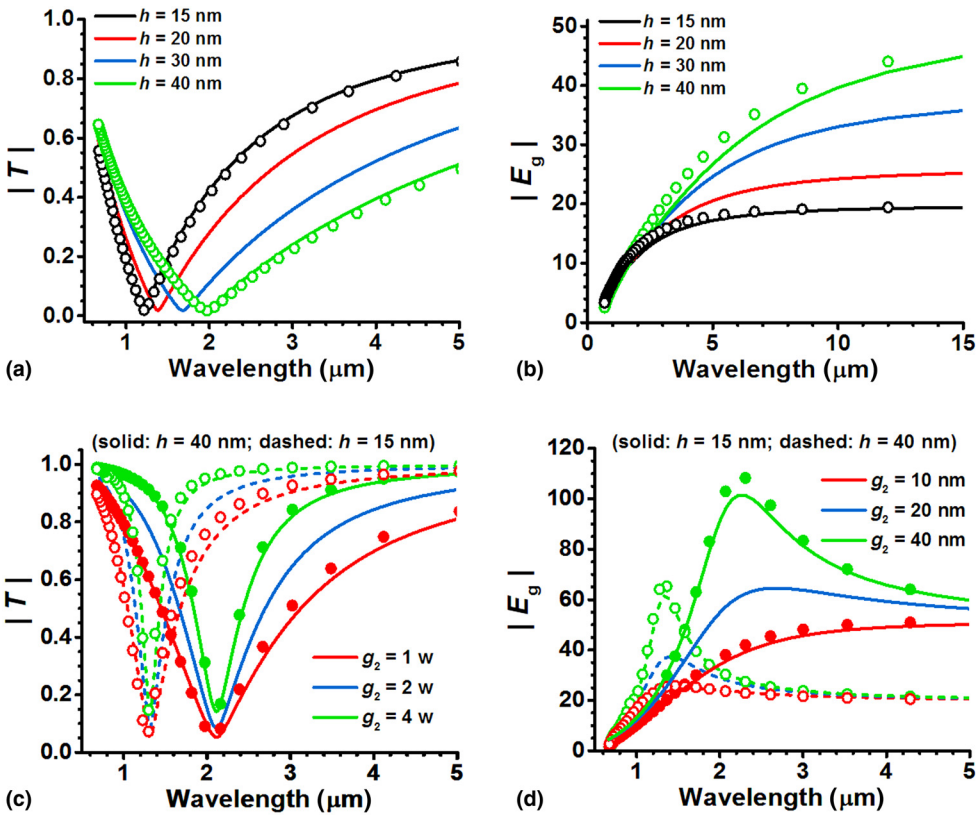

Figure 2. (a) Transmission coefficient and (b) electric field enhancement (inside the MOM heterojunction) against wavelength for the metatronic circuit in Fig. 1(a) in the classical regime (lines, circuit theory calculations; dots, full-wave simulation results). Panels (c) and (d) are similar to (a) and (b), but for the metatronic circuit in Fig. 1(b).

introducing the capacitive element, Z_g, the quality factor, bandwidth, and local field enhancement at resonance can be tailored by varying the g_2/w ratio. Also a larger local field enhancement and Q-factor, which are particularly beneficial for the tunneling-induced nonlinear optical effects, may be obtained with a higher-order nanocircuit. In both types of nanocircuits, the resonance frequency is red-shifted when the metal thickness increases, which also increases the local field strength across the MOM tunnel junction.

In the quantum regime, the proposed nanocircuits can support non-trivial nonlinear optical responses within the MOM tunneling barrier shown in Fig. 3(a). In the general scenario, the voltage applied to the MOM structure is a combination of optical (ac) and dc signals $V(t) = V_{\rm dc} + (1/2)(V_\omega e^{-i\omega t} + c.c)$. From the Tien–Gordon theory of multiphoton-assisted tunneling,[38,39] the time-dependent wavefunction for electrons in metal becomes

$$\psi(\bar{\mathbf{r}}, t) = \psi_0(\bar{\mathbf{r}}, t)\exp\left[-i/\hbar \int^t qV(t')dt'\right] = \psi_0(\bar{\mathbf{r}}, t)\sum_{n=-\infty}^{n=+\infty} J_n\left(qV_\omega/\hbar\,\omega\right)e^{-in\omega t}, \quad (1)$$

where q is the electron charge, $\hbar$ is the reduced Planck constant, $\psi_0(\bar{\mathbf{r}}, t)$ is the unperturbed Schrödinger wavefunction, and $J_n(\cdot)$ is the nth order Bessel function. The modified wavefunction implies that optical signals adiabatically modulate the electron potential energy. The monochromatic electromagnetic field may therefore excite quantum-well virtual states separated from the unperturbed ground state by $\pm n\hbar\omega$, where n corresponds to the number of photons absorbed or emitted, with probability $J_n^2\left(qV_\omega/\hbar\omega\right)$, by an electron at the metal surface. As a result, the time-dependent current is in the form of a Fourier series $I(t) = \sum_{m=0}^{m=+\infty} 1/2\left(I_{m\omega}e^{-im\omega t} + c.c.\right)$,[38,39] where the strengths of current components are given by

$$I_{\rm illum} = \sum_{n=-\infty}^{\infty} J_0^2(\alpha) I_{\rm dark}\left(qV_{dc} + n\hbar\omega\right),$$

$$I_{m\omega} = \sum_{n=-\infty}^{\infty} J_n(\alpha)[J_{n+m}(\alpha) + J_{n-m}(\alpha)]I_{\rm dark}(qV_{dc} + n\hbar\omega), \quad (2)$$

where $\alpha = qV_\omega/\hbar\omega$, $I_{\rm illum}$ and $I_{m\omega}$ represent the dc ($m = 0$) and mth frequency-dependent currents under illumination. At IR and visible wavelengths, where α is typically small, and

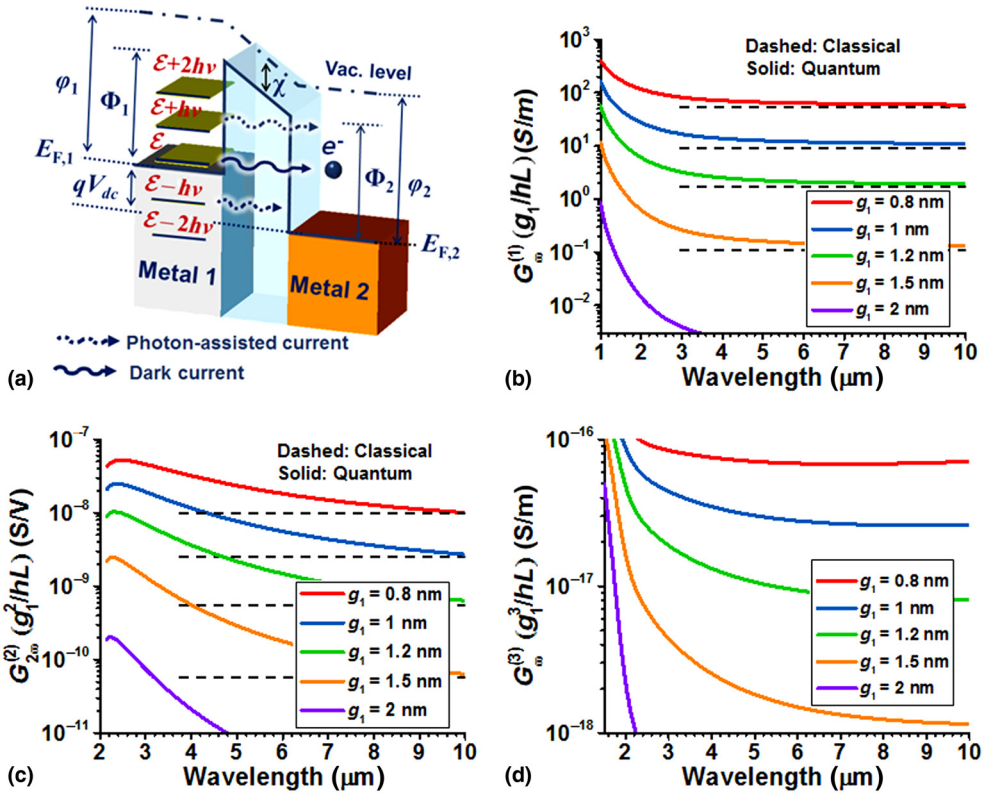

Figure 3. (a) Schematic diagrams of multi-PATin a dissimilar MOM junction. Normalized (b) first-order (linear optical), (c) second-order, and (d) third-order quantum conductance for an Ag–Ta_2O_5–Au junction in Fig. 1(a), with different separations between two metals. Dashed lines in (b) and (d) represent the classical limits $G^{(1)}_{\omega,\text{classic}} g_1/(hL) = (\partial I_{\text{dark}}/\partial V_{\text{dc}})|_{V_{\text{dc}}=0}$ and $G^{(2)}_{2\omega,\text{classic}} g_1^2/(hL) = (1/4)(\partial^2 I_{\text{dark}}/\partial V_{\text{dc}}^2)|_{V_{\text{dc}}=0}$.

below the photoionization threshold, the summations in (2) can be expanded to higher orders in the voltage[33,38,39]:

$$I_{\text{illum}} = I_{\text{dark}}(V_{\text{dc}}) + G_0^{(2)}|V_\omega|^2 + O(\alpha)^4,$$

$$I_\omega = G_\omega^{(1)} V_\omega + G_\omega^{(3)}|V_\omega|^2 V_\omega + O(\alpha)^5,$$

$$I_{2\omega} = G_{2\omega}^{(2)} V_\omega^2 + O(\alpha)^4, \qquad (3)$$

where $G_\omega^{(1)}$ is the quantum conductance in the linear region, and $G^{(0)}$, $G^{(2)}$, $G^{(3)}$, … are nonlinear quantum conductances that arise in an intense optical field. Typically, the contribution of nonlinearities higher than the third-order term can be ignored. The expressions for the linear and nonlinear quantum conductance are derived in the Supplementary Material. The tunneling dark current I_{dark} flowing between two dissimilar metal electrodes can be calculated using the well-known Simmons' quasi-analytical formula[40–42] (see the Supplementary Material for details). Here $G_{2\omega}^{(2)}$ *and* $G_\omega^{(3)}$ are quantum conductances associated with second-harmonic generation (SHG) and TPA nonlinear optical processes, respectively. Here we ignore the third and other high-order harmonics, i.e., $m > 3$, and, in the absence of a dc load line, there is no dc power consumption due to the dark current $I_{\text{dark}}(V_{\text{dc}})$ and the rectified dc current $I_{\text{rect}} \approx G_0^{(2)}|V_\omega|^2$.

Figures 3(b)–3(d) respectively show the spectrum of normalized first-order (linear), second-order, and third-order quantum conductances $G_\omega^{(1)} \times g_1/(wL)$, $G_{2\omega}^{(2)} \times g_1^2/(wL)$, and $G_\omega^{(3)} \times g_1^3/(wL)$ for an Ag–Ta_2O_5–Au junction with different thicknesses of Ta_2O_5 nanofilm. We used the realistic work functions for Ag and Au: $\Phi_{\text{Ag}} = 4.26$ eV and $\Phi_{\text{Au}} = 5.1$ eV, and the static relative permittivity and electron affinity of Ta_2O_5 are $K = 20$ and $\chi = 3.86$ eV.[43] It is seen that linear and nonlinear components of quantum conductance can be greatly enhanced by reducing the Ta_2O_5 thickness, which narrows the potential barrier for electron tunneling and therefore increases the dark current. At high photon energies (or short IR wavelengths), the values of $G_\omega^{(1)}$ and $G_{2\omega}^{(2)}$ are much higher than what expected from purely classic considerations (dashed lines). Moreover, the highly localized electric fields due to the plasmon coupling may enhance any nonlinearity induced inside the nanogap, thus enabling the observation of nonlinear optical effects with reasonable light intensity.

Considering the quantum mechanical PAT effect in MOM nanojunctions, it is also necessary to introduce a shunt tunneling-induced nanoresistor $R_Q^{(1)} = \left(G_\omega^{(1)}\right)^{-1}$ into the lumped circuit model of Figs. 1(b) and 1(c). In addition, a nonlinear nanoresistor $R_Q^{(3)} = \left(G_\omega^{(3)}\left|V_g\right|^2\right)^{-1}$, responsible for the TPA

at intense illumination, could detune the electric field E_g (or voltage V_g) inside the nanogap. Since electric fields are reasonably uniform inside the T_2O_5 layer, according to the circuit model in Fig. 1, the electric field across the T_2O_5 nanofilm is given by $V_g = (Z_{ox}V_\omega)/(Z_{Au} + Z_{Ag} + Z_{ox})$, where the quantum-corrected oxide impedance now becomes $Z_{ox} = i/(\omega C_{ox}) + R_Q^{(1)} + R_Q^{(3)}$, where C_{ox} is the electrostatic capacitance. We note that a transcendental equation must be iteratively solved to evaluate the exact value of local electric field.[13] In addition, the induced nonlinear currents (e.g., $I_{2\omega}$, $I_{3\omega}$, ...) will produce higher-harmonics (e.g., SHG, THG, ...) on both sides of the subwavelength structure in Fig. 1.[14] Fortunately, higher harmonic signals other than the desired one can be filtered out through the design of IR lumped element circuit. For the nanocircuit in Fig. 1(a), the SHG output power can be analyzed using the reduced Norton equivalent circuit in the inset of Fig. 4(a) and is given by:

$$P_{2\omega}^{(2)} = \frac{Z_0}{4}\left|\frac{I_{2\omega}Z_{ox}(2\omega)}{Z_{Cu}(2\omega) + Z_{Al}(2\omega) + Z_{ox}(2\omega) + Z_0/2}\right|^2, \quad (4)$$

where the nonlinear current $I_{2\omega} = G_{2\omega}^{(2)}V_g^2$ is determined by the local electric field $E_g = V_g/g_1$ The SHG conversion efficiency for the device in Fig. 1(b) can be similarly calculated using the Norton equivalent circuit. Considering harmonic balance and power conversation, the incident power P_{inc} must equal the sum of power dissipation at the fundamental and second harmonics: $P_{inc} = |V_0|^2/(2Z_0) \approx (1/2)V_\omega I_\omega^* + (1/2)V_{2\omega}I_{2\omega}^*$, where V_0 is the applied voltage, V and I are the voltage and current flowing through the surface impedance of the periodic MOM-superlattice structure. Figs. 4(a) and 4(b) show the spectral SHG conversion efficiency $\eta_{shg} = P_{2\omega}^{(2)}/P_{inc}$ at the second-harmonic frequency for the structure in Fig. 1(a), varying the metal thickness; here the pump intensity is 40 MW/cm^2. Figs. 4(a) and 4(b) reveal that in the long-wavelength region the SHG efficiency increases with frequency, since in the quantum regime $G_{2\omega}^{(2)}$, as seen in Fig. 3(c), becomes larger at higher photon energy. However, the SHG efficiency saturates in the vicinity of the cut-off wavelength of the circuit. We should note that the nanocircuit may be further optimized to accomplish a dual resonance at the fundamental and second

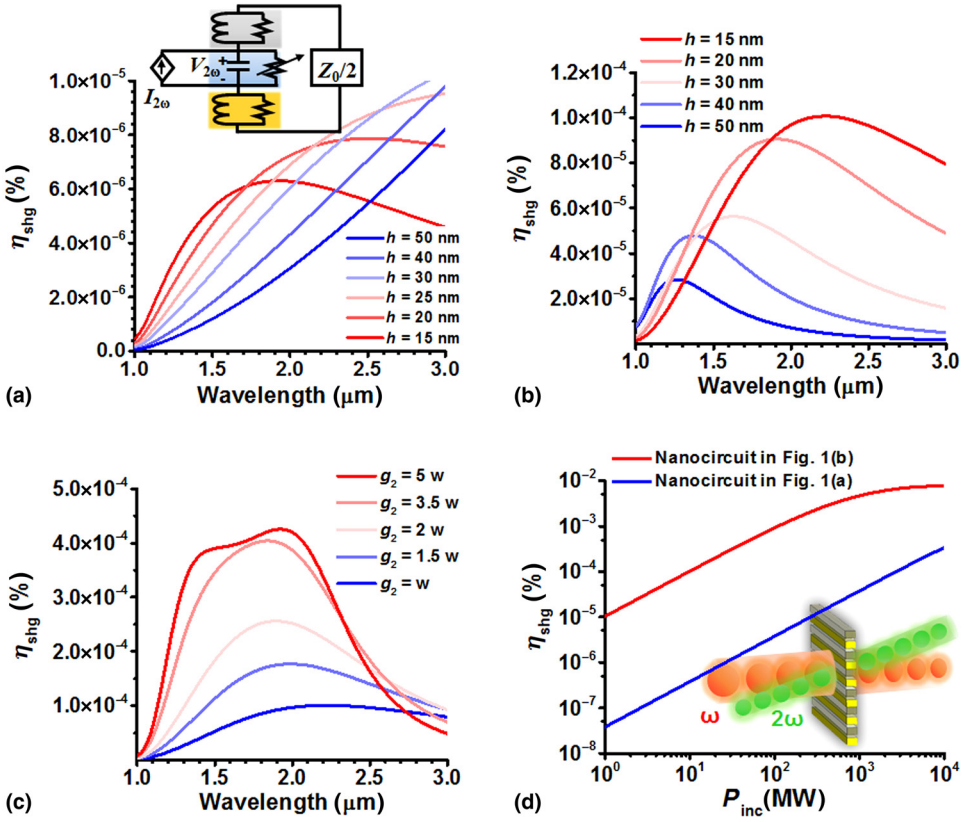

Figure 4. SHG conversion efficiency for (a) the metatronic circuit in Fig. 1(a) with different metal thicknesses (varying Z_{Au} and Z_{Ag}), and the metatronic circuit in Fig. 1(b), with (b) different thicknesses of metal (varying Z_{Au} and Z_{Ag}) and (c) different widths of air gap (varying Z_g). The inset of (a) shows the reduced equivalent circuit model at the second-harmonic frequency. (d) SHG conversion efficiency against the intensity of incident radiation for the metatronic circuits in Figs. 1(a) and 1(b).

harmonics (e.g., by introducing more lumped elements), which may accordingly increase the SHG conversion efficiency.

From Figs. 4(a) and 4(b), we see that the higher-order circuit in Fig. 1(b) can offer a significantly larger SHG conversion efficiency, due to the higher local field enhancement inside the MOM junction, as expected from the classical circuit analysis in Figs. 2(b) and 2(d). In addition, a thicker metal layer may lead to a larger SHG conversion efficiency, since it induces a stronger optical field across the tunnel junction [see Figs. 2(b) and 2(d)]. We also study the effect of air-gap width on the SHG conversion efficiency. Figure 4(c) is similar to Fig. 4(b), but for different air-gap widths g_2. We found that the SHG output power can be increased by enlarging the air-gap width, while the peak SHG frequency remains unchanged (~2 μm). Figure 4(d) shows the SHG conversion efficiency against the illumination power for the two different types of nanocircuits in Fig. 1, which share similar dimensions $g_1 =$ 0.8 nm, $h = 50$ nm, and $L = 10$ nm, and the input laser wavelength $\lambda_0 = 3.2$ μm; the nanocircuit design of Fig. 1(b) has an air gap $g_2 = 5\,w$ and $w \ll \lambda_0$. It is seen that by designing complicated higher-order circuit, the SHG output power, when compared with the pure MOM-superlattice structure in Fig. 1(a), can be greatly improved. Intuitively, the SHG conversion efficiency grows with increasing illumination power. However, the conversion efficiency saturates at high irradiance levels due to the increasing importance of the TPA effect, which leads to the power dissipation and limits the field enhancement. This saturation effect for SHG output power is more obvious for the higher-order nanocircuit [i.e., Fig. 1(b)], where the field-intensity-dependent TPA effect is boosted by the stronger localized electric fields inside the MOM nanojunction. Assuming a nonlinear optical thin film with thickness of 10 nm and relative permittivity $\varepsilon = 4.4$ (similar to the length and relative permittivity of Ta_2O_5 nanofilm), a very high equivalent second-order susceptibility (The SHG conversion efficiency of a nonlinear optical thin film can be calculated as calculated $\eta^{SHG} = \tanh^2[\zeta]/\mathrm{sech}^2[0]$, where $\zeta = x/l$ is the normalized distance parameter, x is the distance from the crystal interface and $l = [2(\varepsilon(\omega))^2\varepsilon(2\omega)\varepsilon_0 c^3/I_0]^{1/2}/(\omega\chi^{(2)})$), $\chi^{(2)}$ up to 1.8×10^4 pm/V can be obtained at the SHG peak in Fig. 4(c) ($\eta_{2\omega} \approx 4 \times 10^{-4}$ %) at 40 GW/cm^2. Such value is at least four-orders larger than conventional nonlinear optical materials.[44].

Finally, we apply these concepts to design a TPA-based nanoswitch, whose intensity-dependent nonlinear response may be used to modulate the intensity of transmitted light (i.e., resistive switching). Here we use the same nanocircuit in Fig. 1(b), with $g_1 = 0.8$ nm, $g_2 = 5\,w$, and $L = 8$ nm. Figures 5(a) and 5(b) report the transmittance spectrum under various illumination intensities, for metal thickness $h = 60$ and 40 nm. The inset of Fig. 5(b) illustrates the onset and offset of such device, realized with the variation of input intensity. By increasing the incident irradiance, the transmittance can be largely modulated, due to the enhanced TPA effects and its enabled nonlinear self-modulation in the quantum resistance, $\mathrm{Re}[Z_{ox}]$. The inset of Fig. 5(b) illustrates the onset and offset of such device, realized by varying the input intensity. Under high-input intensities, the MOM nanojunction may absorb considerable power, leading to the deterioration of local field enhancement, as well as a variation in transparency and absorption. Moreover, the peak resonance with largest modulation depth can be readily tailored by designing the nanocircuit, as seen in Figs. 5(a) and 5(b). Unlike bistable switching devices based on reactive nonlinear responses (i.e., $\mathrm{Re}[\chi^{(2)}]$ or n_2),[13–21,45,46] this nonlinear resistive switching can offer significantly improved bandwidth, of interest for all-optical switching.

In summary, we have introduced here nonlinear IR metatronic elements as building blocks for frequency and amplitude modulation, analogous to RF diodes, despite their nanosize feature. In this work, we focused on second-harmonic generation [which shows a high equivalent $\chi^{(2)}$ of 1.8×10^4 pm/V] and

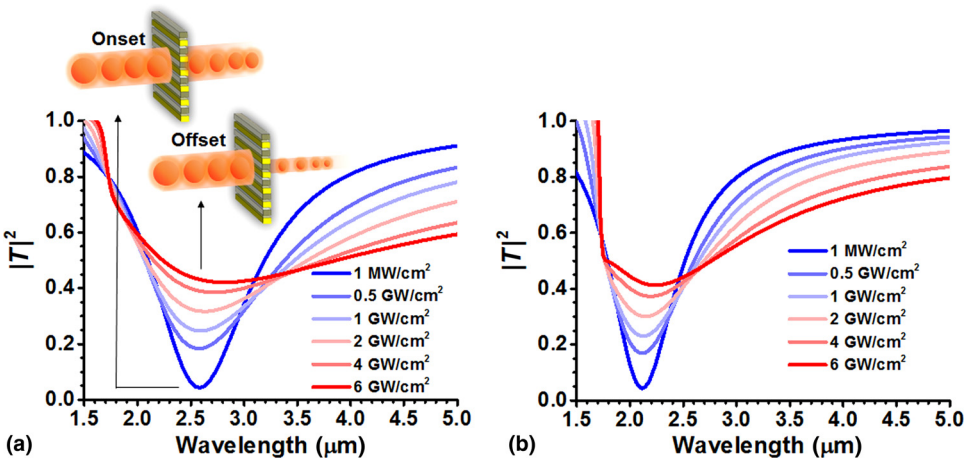

Figure 5. Transmittance spectrum for the metatronic circuit in Fig. 1(b), with metal thickness of (a) $h = 60$ nm and (b) $h = 40$ nm, under different illumination intensities.

broadband self-amplitude modulation of transmittance via nonlinear two-photon absorption. These devices were designed and analyzed using the circuit concept, and they may be applied to novel IR mixers, transponders, and switches. We envision that the enhanced optical nonlinearities due to the interplay between PAT and plasmon coupling within atomic-scale MOM-superlattices, common in metamaterial and metatronic-circuit topologies,[3,4] may provide tremendous potential in the design of novel nonlinear nanophotonic and nano-optical devices.

Supplementary materials

For supplementary material for this article, please visit http://dx.doi.org/10.1557/mrc.2015.75

Acknowledgments

A.A. acknowledges support from the Air Force Office of Scientific Research with grant No. FA9550-13-1-0204, and the Office of Naval Research with MURI grant No. N00014-10-1-0942.

References

1. N. Engheta, A. Salandrino, and A. Alù: Circuit elements at optical frequencies: nanoinductors, nanocapacitors, and nanoresistors. *Phys. Rev. Lett.* **95**, 095504 (2005).
2. N. Engheta: Circuits with light at nanoscales: optical nanocircuits inspired by metamaterials. *Science* **317**, 1698 (2007).
3. Y. Sun, B. Edwards, A. Alù, and N. Engheta: Experimental realization of optical lumped nanocircuits at infrared wavelengths. *Nat. Mater.* **11**, 208–212 (2012).
4. H. Caglayan, S.H. Hong, B. Edwards, C.R. Kagan, and N. Engheta: Near infrared metatronic nanocircuits by design. *Phys. Rev. Lett.* **111**, 073904 (2013).
5. N. Engheta: From radio-frequency circuits to optical nanocircuits. *IEEE Microw. Mag.* **13**, 100–113 (2012).
6. A. Alù and N. Engheta: Optical metamaterials based on optical nanocircuits. *Proc. IEEE* **99**, 1669–1681 (2011).
7. A. Alù and N. Engheta: Tuning the scattering response of optical nanoantennas with nanocircuit Loads. *Nat. Photonics* **2**, 307 (2008).
8. M. Schnell, A. García-Etxarri, A.J. Huber, K. Crozier, J. Aizpurua, and R. Hillenbrand: Controlling the near-field oscillations of loaded plasmonic nanoantennas. *Nat. Photonics* **3**, 287–291 (2009).
9. N. Liu, F. Wen, Y. Zhao, Y. Wang, P. Nordlander, N.J. Halas, and A. Alù: Individual nanoantennas loaded with three-dimensional optical nanocircuits. *Nano Lett.* **13**, 142–147 (2012).
10. J.A. Fan, C. Wu, K. Bao, J. Bao, R. Bardhan, N.J. Halas, V.N. Manoharan, P. Nordlander, G. Shvets, and F. Capasso: Self-assembled plasmonic nanoparticle clusters. *Science* **328**, 1135–1138 (2010).
11. J. Shi, S. Elias, F. Monticone, Y. Wu, D. Ratchford, X. Li, and A. Alù: Modular assembly of optical nanocircuits. *Nature Commun.* **5**, 3896 (2014).
12. A. Goldsmith: *Wireless Communications* (Cambridge University Press, New York, 2005).
13. P.Y. Chen, M. Farhat, and A. Alù: Bistable and self-tunable negative-index metamaterial at optical frequencies. *Phys. Rev. Lett.* **106**, 105503 (2011).
14. P.Y. Chen and A. Alù: Subwavelength imaging using phase-conjugating nonlinear nanoantenna arrays. *Nano Lett.* **11**, 5514 (2011).
15. P.Y. Chen and A. Alù: Optical nanoantenna arrays loaded with nonlinear materials. *Phys. Rev. B* **82**, 235405 (2010).
16. P.Y. Chen, C. Argyropoulos, and A. Alù: Enhanced nonlinearities using plasmonic nanoantennas. *Nanophotonics* **1**, 221 (2012).
17. P.Y. Chen and A. Alù: A terahertz photomixer based on plasmonic nanoantennas coupled to a graphene emitter. *Nanotechnology* **24**, 455202 (2013).
18. U.K. Chettiar and N. Engheta: Optical frequency mixing through nanoantenna enhanced difference frequency generation: metatronic mixer. *Phys. Rev. B* **86**, 075405 (2012).
19. P.Y. Chen, C. Argyropoulos, G. D'Aguanno, and A. Alù: Enhanced second-harmonic generation by metasurface nanomixer and nanocavity. *ACS Photonics* **2**, 1000–1006 (2015).
20. R.E. Noskov, P.A. Belov, and Y.S. Kivshar: Subwavelength modulational instability and plasmon oscillons in nanoparticle arrays. *Phys. Rev. Lett.* **108**, 093901 (2012).
21. I.S. Maksymov, A.E. Miroshnichenko, and Y.S. Kivshar: Actively tunable bistable optical Yagi-Uda nanoantenna. *Opt. Express* **20**, 8929–8938 (2012).
22. M. Kauranen and A.V. Zayats: Nonlinear plasmonics. *Nat. Photonics* **6**, 737–748 (2012).
23. H. Harutyunyan, G. Volpe, R. Quidant, and L. Novotny: Enhancing the nonlinear optical response using multifrequency gold-nanowire antennas. *Phys. Rev. Lett.* **108**, 217403 (2012).
24. A.M. Mahmoud, A.R. Davoyan, and N. Engheta: All-passive nonreciprocal metastructure. *Nat. Commun.* **6**, 8359 (2015).
25. U.K. Chettiar and N. Engheta: Metatronic transistor amplifier. *Phys. Rev. B* **92**, 165413 (2015).
26. J. Zuloaga, E. Prodan, and P. Nordlander: Quantum description of the plasmon resonances of a nanoparticle dimer. *Nano Lett.* **9**, 887 (2009).
27. D.C. Marinica, A.K. Kazansky, P. Nordlander, J. Aizpurua, and A. G. Borisov: Quantum plasmonics: nonlinear effects in the field enhancement of a plasmonic nanoparticle dimer. *Nano Lett.* **12**, 1333 (2012).
28. G. Hajisalem, M.S. Nezami, and R. Gordon: The dark side of plasmonics. *Nano Lett.* **14**, 6651 (2014).
29. J.W. Haus, D. de Ceglia, M.A. Vincenti, and M. Scalora: Quantum conductivity for metal- insulator-metal nanostructures. *J. Opt. Soc. Am. B* **31**, 259 (2014).
30. J.W. Haus, D. de Ceglia, M.A. Vincenti, and M. Scalora: Nonlinear quantum tunneling effects in nano-plasmonic environments. *J. Opt. Soc. Am. B* **31**, A13 (2014).
31. M.L. Brongersma, N.J. Halas, and P. Nordlander: Plasmon-induced hot carrier science and technology. *Nat. Nanotechnol.* **10**, 25–34 (2015).
32. P.Y. Chen and M. Farhat: Modulatable optical radiators and metasurfaces based on quantum nanoantennas. *Phys. Rev. B* **91**, 035426 (2015).
33. S. Grover and G. Moddel: Applicability of metal/insulator/metal (MIM) diodes to solar rectennas. *IEEE J. Photovolt.* **1**, 78 (2011).
34. P.B. Johnson and R.W. Christy: Optical constants of the noble metals. *Phys. Rev. B* **6**, 4307 (1972).
35. P.R. West, S. Ishii, G.V. Naik, N.K. Emani, V.M. Shalaev, and A. Boltasseva: Searching for better plasmonic materials. *Laser Photonics Rev.* **4**, 795–808 (2010).
36. Refractive index database (http://refractiveindex.info/)
37. CST Microwave Studio (http://www.cst.com)
38. P.K. Tien and J.P. Gordon: Multiphoton process observed in the interaction of microwave fields with the tunneling between superconductor films. *Phy. Rev.* **129**, 647 (1963).
39. J.R. Truker: Quantum limited detection in tunnel junction mixers. *IEEE J. Quantum Electron* **15**, 1234 (1979).
40. J.G. Simmons: Generalized formula for the electric tunnel effect between similar electrodes separated by a thin insulating film. *J. Appl. Phys.* **34**, 1793 (1963).
41. J.G. Simmons: Electric tunnel effect between dissimilar electrodes separated by a thin insulating film. *J. Appl. Phys.* **34**, 2581 (1963).
42. J.G. Simmons: Generalized thermal J-V characteristic for the electric tunnel effect. *J. Appl. Phys.* **35**, 2655 (1964).
43. S. Grover and G. Moddel: Engineering the current–voltage characteristics of metal–insulator–metal diodes using double-insulator tunnel barriers. *Solid State Electron.* **67**, 94–99 (2012).
44. R.W. Boyd: *Nonlinear Optics*, 3rd ed. (Academic Press, New York, 2008).
45. C. Argyropoulos, P.Y. Chen, G. D'Aguanno, N. Engheta, and A. Alù: Boosting optical nonlinearities in ϵ-near-zero plasmonic channels. *Phys. Rev. B* **85**, 045129 (2012).
46. C. Argyropoulos, P.Y. Chen, F. Monticone, G. D'Aguanno, and A. Alù: Nonlinear plasmonic cloaks to realize giant all-optical scattering switching. *Phys. Rev. Lett.* **108**, 263905 (2012).